AGU PUBLICATIONS

Radio Science

RESEARCH ARTICLE
10.1002/2013RS005263

Key Points:
- Frequently used theoretical profilers for topside ionosphere are evaluated
- Topside profile shape dependence on various physical drivers is investigated
- Density peak characteristics provide reliable criteria for selecting a profiler

Correspondence to:
T. Verhulst,
tobias.verhulst@meteo.be

Citation:
Verhulst, T., and S. M. Stankov (2014), Evaluation of ionospheric profilers using topside sounding data, *Radio Sci.*, *49*, 181–195, doi:10.1002/2013RS005263.

Received 4 JUL 2013
Accepted 15 FEB 2014
Accepted article online 24 FEB 2014
Published online 18 MAR 2014

Evaluation of ionospheric profilers using topside sounding data

T. Verhulst[1] and S. M. Stankov[1]

[1]Royal Meteorological Institute (RMI), Brussels, Belgium

Abstract An operational system for deducing and imaging the vertical distribution of the electron density in the local ionosphere has been recently developed. The electron density profile is deduced from combined ground-based measurements of the total electron content, ionospheric vertical incidence soundings, and empirically obtained values of the O^+-H^+ ion transition height. The topside profile is permitted to take one of several forms: Exponential, Chapman, or Epstein. An evaluation of the above mentioned ionospheric profilers is needed in order to determine which one of them provides the best representation of the current ionospheric conditions. For this purpose, we use electron density profiles obtained from ionograms recorded by the topside sounders onboard the Alouette and ISIS satellites. Every profile has been fitted with each of the above mentioned theoretical ionospheric profilers and the corresponding approximation errors calculated. The results have been analyzed with respect to local time, geomagnetic latitude, season, magnetic and solar activity, ion transition height, and the ionospheric density peak characteristics. It has been found that, in the majority of cases, the best fit is provided by the exponential profiler, followed by the Chapman profiler. Also, while some influence of the underlying physical drivers on the topside electron density profile is detected, it is the use of ionospheric characteristics that offers more reliable selection criteria for the most appropriate profiler.

1. Introduction

One of the most important characteristics of the ionosphere-plasmasphere system is the plasma scale height. The scale height has the dimension of length and is a critical property of any atmosphere. The plasma scale height is defined [*Hargreaves*, 1992] as $H_P = kT_P/m_i g$, where m_i is the ion mass, $T_P = T_i + T_e$ is the plasma temperature, T_i and T_e are the ion and electron temperatures, and k is the Boltzmann constant (1.380658×10^{-23} J/K). Similarly, the scale height can be defined for each ion or neutral constituent (Figure 1a). In practice, the vertical scale height can be approximately deduced as the vertical distance in which the concentration changes by a factor of an exponent ($e \approx 2.7182$). The scale height value represents the density gradient—the "sharper" the peak electron density, the smaller is the scale height.

Since many ionospheric phenomena leave their signature on the scale height, investigations of its behavioral patterns may answer some open questions in ionospheric physics, particularly those related to ionosphere composition and dynamics. Understanding the scale height behavior is of particular importance to several scientific and technical applications. For many years, simple ionospheric profilers, such as the Exponential, Chapman, and Epstein layers [*Rawer*, 1988, 1993; *Stankov et al*., 2003, and references therein], have been used to model the topside ionosphere. For example, these profilers were used in empirical models, such as the International Reference Ionosphere (IRI) and the NeQuick model [*Bilitza*, 2001; *Depuev and Pulinets*, 2004; *Coïsson et al*., 2006]. Also, in the software for inversion of ionograms in modern digital ionosondes, the Epstein formulae are applied to complement the deduced bottomside electron profile with a topside profile [*Reinisch*, 1996; *Reinisch and Huang*, 2001; *Reinisch et al*., 2005, 2007]. However, because the topside scale height is unknown, it is assumed that the scale height above the ionospheric F_2 layer peak density height equals the scale height just below the peak height; this is a strong assumption which is not always correct. There are also density reconstruction techniques, the radio occultations in particular, that could significantly benefit from the knowledge of the topside ionospheric scale height, at least as a source of an educated initial guess.

An operational system for deducing and imaging the vertical distribution of the electron density in the local ionosphere (LIEDR–Local Ionospheric Electron Density profile Reconstruction) has been recently developed

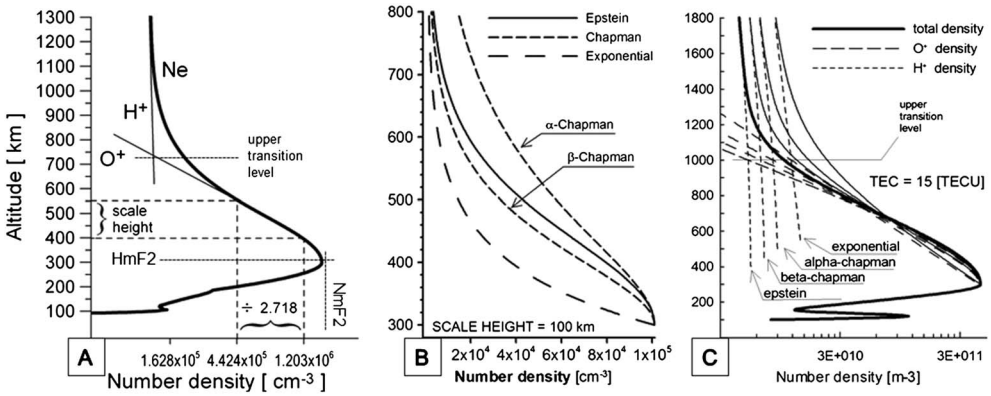

Figure 1. (a) Ion and electron density profile characteristics. Comparison between vertical density profiles obtained with basic analytical models for a given fixed scale height of (b) 100 km and (c) TEC of 15 TECU (after figures 2 and 5 in *Stankov et al*., 2003).

[*Stankov et al*., 2011]. At a given location, the vertical electron density profile is deduced from local ground-based measurements of the total electron content (TEC), ionospheric vertical incidence soundings, and empirically obtained values of the upper O^+-H^+ ion transition height/level (UTL). The retrieval of the corresponding vertical electron density distribution is performed in two main stages: construction of the bottomside electron profile (below the ionospheric F_2 layer peak density height, h_mF_2) and construction of \the topside profiles (above h_mF_2). The topside profile is permitted to take one of several forms: Exponential, α-Chapman, β-Chapman, or Epstein. The system acquires and promptly processes the incoming measurements, computes the full-height ionospheric electron density profile, and displays the resulting profilograms. LIEDR is designed to operate in continuous real-time mode for service applications and to provide historical data and plots for research applications and further developments of the system. It is currently in operation at the Royal Meteorological Institute (RMI) Geophysical Centre in Dourbes (50.1°N, 4.6°E).

Evaluation of the above mentioned different forms of topside profiles is needed in order to find out which of them provides the best representation of the current ionospheric conditions. For this purpose, we use electron density profiles measured by the topside sounders onboard the Alouette and ISIS satellites [*Jackson and Warren*, 1969; *Jackson*, 1969a, 1988; *Jackson et al*., 1980; *Bilitza et al*., 2003]. Every profile has been fitted with each of the theoretical ionospheric profilers, and the corresponding approximation errors were calculated. The approximation results are analyzed with respect to external factors (local time, geomagnetic latitude, season, and solar activity), as well as the key characteristics of the topside ionosphere (the ionospheric F_2 layer peak density height, N_mF_2, peak height, h_mF_2, and the upper transition level). Related work has been done, for example using the data from ISIS 2 and IK 19 [*Fonda et al*., 2005]. However, the aim of the current work is to find the appropriate topside profiler for given conditions, rather than a profile that fits best on average.

The paper is organized as follows: First, the evaluation method is detailed, including formulae for calculation of the scale heights and the integrated errors. Next, the database is presented with particular focus on the data processing and cleaning. Evaluation results will be presented in the next part. The paper will conclude with a discussion of the results and an outlook for possible applications of the analyzed profilers for improvements in the LIEDR system.

2. Method

2.1. Calculation of the Scale Heights

Here the method is described to calculate the scale height for the different profiles from the experimental data. Notational convention: $N(h)$ and N_p indicate the density at height h and at the peak. $n(h)$ and n_p are used to indicate the logarithms of the densities. h_p is the height of the peak, and h_{p+1} is the first measured point above the peak.

By calculating the scale height as described in this section, a good fit is assured in the region close to the peak. This is the region that contributes the most to the integrated error, because of the larger densities, and is therefore the most important to get a good fit for. This is also the region where the difference in shape between possible model curves is the clearest. Another possible procedure to calculate the topside scale height is to utilize the linear regression method using points in the middle of the topside ionosphere [*Marinov et al.*, 2004; *Kutiev and Marinov*, 2007]. This procedure has the advantage that it can be used even when the measured profiles contain a lot of noise, because the regression can diminish its effect by using more data points. However, this method cannot be used here because the goal of this work is to distinguish between the differently shaped curves, and to be able to do so, a good fit near the top of the profile is needed. This is not provided by the regression method.

The electron density profiles resulting from the use of the four different models (profilers) are shown in Figure 1. Figure 1b shows the results when using the same scale height, while Figure 1c shows the electron density profiles, each obtained with a different profiler using a different scale height but the same topside TEC value (integrated electron density above the F_2 peak).

If the density profile is exponential, the density at height h is given by

$$N(h) = N_p \exp\left(-\frac{h - hp}{H_{\exp}}\right). \tag{1}$$

For the scale height, $H_{\exp}$, it immediately follows that

$$H_{\exp} = \frac{h_p - h_{p+1}}{n(h_{p+1}) - n_p}. \tag{2}$$

The Epstein profile is given by

$$N(h) = N_p \operatorname{sech}^2\left(\frac{h - h_p}{2H_{\text{eps}}}\right). \tag{3}$$

Calculating the scale height, H_{eps}, from this gives

$$H_{\text{eps}} = (h_{p+1} - h_p) / 2\operatorname{arcsech}\left[\exp\left(-\frac{n(h_{p+1}) - n_p}{2}\right)\right] = \tag{4}$$

$$= (h_{p+1} - h_p) \Big/ 2\ln\left[\exp\left(\frac{n_p - n(h_{p+1})}{2}\right) + \sqrt{\exp(n_p - n(h_{p+1})) - 1}\right]. \tag{5}$$

For the Chapman profile, the density is

$$N(h) = N_p \exp\left\{c\left[1 - \frac{h - h_p}{H_{(\alpha,\beta)}} - \exp\left(-\frac{h - h_p}{H_{(\alpha,\beta)}}\right)\right]\right\}, c = \begin{cases} 0.5, \text{Chapman-}\alpha \\ 1.0, \text{Chapman-}\beta \end{cases}. \tag{6}$$

Calculating the scale height, $H_{(\alpha,\beta)}$, from this gives

$$H_{(\alpha,\beta)} = (h_{p+1} - h_p) \Big/ \left\{1 - \frac{n(h_{p+1}) - n_p}{c} + \mathrm{W}\left[-\exp\left(\frac{n(h_{p+1}) - n_p}{c}\right)\right]\right\}. \tag{7}$$

Here $W(z)$ is the Lambert-W function that can be evaluated by iterating the following [*Corless et al.*, 1996]:

$$W_{j+1}(z) = W_j(z) + \left[W_j(z)\exp(W_j(z)) - z\right] \Big/ \left\{(1 + W_j(z))\exp(\mathrm{W}_j(z)) - \frac{(W_j(z) + 2)\left[W_j(z)\exp(\mathrm{W}_j(z)) - z\right]}{2(1 + W_j(z))}\right\}. \tag{8}$$

The most straightforward way to calculate the scale height would be to find the height at which the density is a factor $1/e$ less than the peak density by using linear interpolation between the data points. However, this method produces only one scale height and is a source of systematic bias favoring the exponential profile. Figure 2 shows a profile that is best fitted by an α-Chapman profiler. When using the same scale height, calculated using equation (2), for both the exponential and α-Chapman profiles, the exponential profiler gives a better result. This is to be expected, because those profilers result in very different curves when the same scale height is used for both, as can be seen in Figure 1b. In reality, for each of the four profilers, the scale height calculated specifically for that profiler has to be used. Those scale heights are

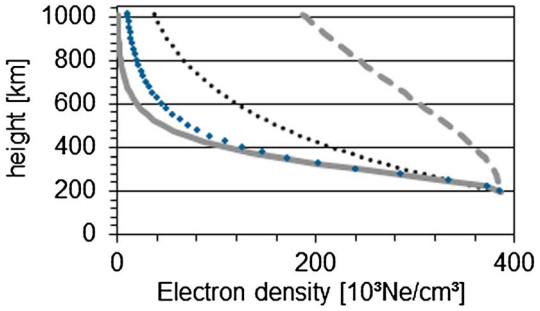

Figure 2. Comparison of different shapes with different scale heights, all fitted to a measured density profile. The blue diamonds show the measured densities, and the lines are the fitted profiles (the dotted line is the exponential shape; the solid one is the α-Chapman shape; and the dashed line is the α-Chapman profile calculated using the exponential scale height).

given by equations (2), (5), and (7). This method has the additional advantage of being easy to adapt for using varying scale heights.

2.2. Calculation of the Upper Transition Level

The upper transition level is defined as the height at which the O^+ and H^+ ion concentrations are equal. Earlier work has been done developing methods to extract this transition level from the measured profiles, provided that the profile reaches to high enough altitudes [*Titheridge*, 1976; *Webb et al*., 2006]. These techniques have the advantage of directly fitting physical models to the measured profiles. However, we use a different procedure [*Marinov et al*., 2004; *Kutiev and Marinov*, 2007] calculating first an extrapolated O^+ density profile and comparing it with the measured electron density profile. Thus, the upper transition level is determined as the height at which the measured electron density is twice the one predicted by this extrapolation. This method can be used to discard profiles that do not reach the ion transition height.

2.3. Calculation of the Integrated Errors

To estimate how well the four different profiles fit the measured densities, the following integrated error is defined

$$Er_i = \ln\left(\int_{h_p}^{TH} |n(h) - n_i(h)|dh\right), \tag{9}$$

where h_p is the height of the F_2 peak, and *TH* is the transition level. The logarithm of the integral is used in order to keep the values confined to a range that is both manageable by the numerical procedures and more convenient for graphical presentation. The index *i* indicates which of the four possible profiles is used. $n(h)$ is the measured Alouette/ISIS electron-density profile based on earlier hand scaling, and $n_i(h)$ is the predicted profile for the shape indicated by *i*. Thus, the predicted density is $n_{exp}(h)$ if the profile is exponential, $n_\alpha(h)$ if the shape is α-Chapman, and so on. This integrated error depends on the total thickness of the ionosphere and can therefore only be used to compare different theoretical shapes of the density profile for one measured profile. It should not be used to compare the errors for different measured profiles as the thickness might be different between them. Because the densities are only measured at discrete points, the integral in equation (9) has to be approximated by a summation over the measured points (h_t is the measured point closest to *TH*):

$$Er_i = \ln\left[|n(h_t) - n_i(h_t)|\cdot\frac{h_t - h_{t+1}}{2} + \sum_{j=2}^{N-1}\left(|n(h_j) - n_i(h_j)|\cdot\frac{h_{j-1} - h_{j+1}}{2}\right) + |n(h_p) - n_i(h_p)|\cdot\frac{h_{p-1} - h_p}{2}\right]. \tag{10}$$

Here $h_t \equiv h_1$ is the measured point closest to *TH*; $h_P \equiv h_N$ is the height of the F_2 peak, assumed to be at the lowest measured point; and *N* is the number of measurements in the profile. The above expression can be simplified if the measured points are equidistant, but for most profiles, this is not the case.

3. Data Processing and Cleaning

This work utilizes topside sounder data from the Alouette 1 and 2 and ISIS 1 and 2 satellites [*Jackson and Warren*, 1969; *Jackson et al*., 1980; *Jackson*, 1988]. The database is available for download from the National Space Science Data Center and comprises profiles obtained from the measured analog ionograms by different groups [*Bilitza et al*., 2003; *Benson*, 2010]. There are 176,662 density profiles, 85,772 from Alouette 19,301 from Alouette 2, 28,953 from ISIS 1, and 42,596 from ISIS 2. It is important to realize that the temporal and spatial distribution of the data is very irregular, due to the fact that the measurements come from different satellites, traveling on different orbits and during different time periods. We describe here briefly the

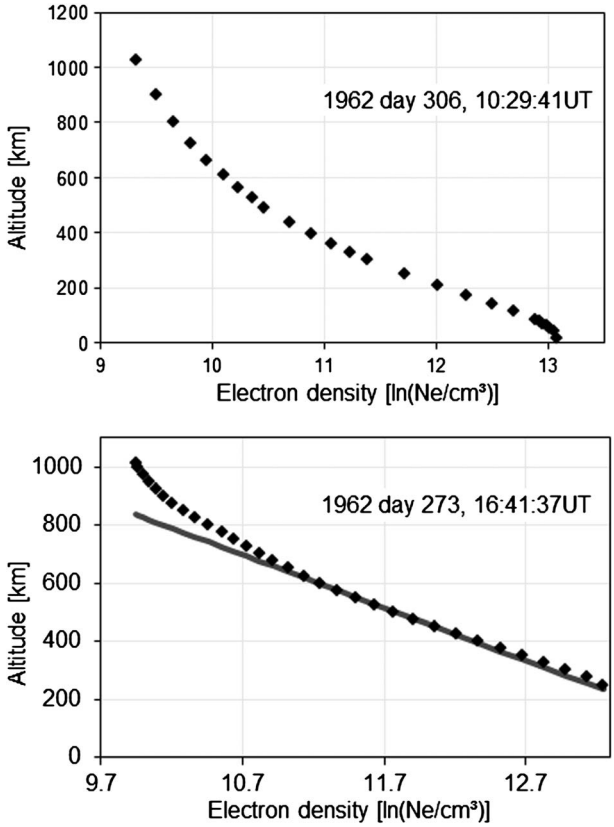

Figure 3. Electron density profiles illustrating different reasons for the exclusion of profiles from the data. (top) Profile with densities measured down to 17 km, which is physically impossible. (bottom) Profile together with the extrapolated O^+ density. Clearly, the satellite was below *TH* at the moment this profile was measured. Both of these profiles were obtained by Alouette 1.

most important points in the data preprocessing that are relevant to this paper. A more detailed description of the data cleaning methods, as well as an overview of possible biases due to the irregular distribution of the data, are given in *Verhulst and Stankov* [2013].

It is clear that, for some of the profiles, errors have been generated either during the satellite measurements or at some stage during the consequent data processing (although the scaling itself is, in this work, taken to be perfect; i.e., we do not take into account possible uncertainties in the positions of the points in the electron density profiles, only that the original ionogram might display some errors) [*Verhulst and Stankov*, 2013]. For example, Figure 3 (top) shows an electron density profile for which the lowest measured point is at a height of only 17 km. Such profiles are impossible to exist, and their use may jeopardize the validity of some particular studies. The number of profiles that reach altitudes which are clearly impossible is very small. However, a major problem is that the lowest point in a profile can be at an altitude that is possible in principle, while still being wrong. When comparing the h_mF_2 values obtained from topside ionosondes—measured above an ionosonde station—with the values measured by the ground-based ionosonde, the value obtained from the satellite-based sounder is typically 10 km too high [*Jackson*, 1969b; *Benson*, 2010] (this is the typical value, not the extreme). This is especially problematic for the comparison of possible profile shapes because it is in the topside ionosphere close to the region where the difference between the possible shapes is most obvious. To avoid both these types of errors, in our analysis, only those profiles were used for which the measured peak density is within 50 km of the peak height predicted by the International Reference Ionosphere model [*Bilitza*, 2001; *Bilitza and Reinisch*, 2008]. This procedure will result in disregarding some profiles that are correct, since larger deviations from the IRI model are entirely possible. However, for this particular study, we decided that it was preferable to use rather strict criteria for data selection in order to assure that all erroneous profiles are removed. Over 68,000 profiles do not meet this criterion and are therefore disregarded in the further analysis. Apart from profiles that are rejected because of an error, there are also profiles that, while correct in themselves, cannot be used because at the time of the measurement, the satellite was below the transition level. These profiles are discarded to avoid possible biases if the integrated errors for the different profiles cannot be computed across the total thickness of the ionosphere. Figure 3 (bottom) gives an example of such a profile. Only 32,583 profiles are left after disregarding those for which no transition level could be determined [*Verhulst and Stankov*, 2013].

One of the advantages of this database is that it covers more than one full solar cycle and consequentially a broad range of solar activities. In Table 1, it can be seen that all values of $F_{10.7}$ are covered from 60 to above 200. The $F_{10.7}$ solar activity index is not included in the database with satellite data but is looked up in the Space Physics Interactive Data Resource (SPIDR) database [*O'Loughlin*, 1997]. However, in the database, there are 1456 profiles for which no value for the $F_{10.7}$ flux at the time of measurement is available. These are from

Table 1. Number of Profiles, Sorted According to Level of Solar Activity ($F_{10.7}$ Index Used), That are Available in the Different Databases Used for the Study

	Alouette 1A	Alouette 1B	Alouette 1C	Alouette 2	ISIS 1	ISIS 2
Total	15,708	43,548	26,040	9,303	38,955	42,595
Unsorted[a]	612	723	56			
60–80	5,410	22,910	13,411	857	608	4,394
80–100	9,686	18,643	70,76	1,293	531	8,344
100–120		1,272	3,189	2,114	3,896	13,401
120–140			1,511	1,867	12,204	12,950
140–160			797	1,537	10,980	2,250
160–180				666	5,989	875
180–200				243	2,377	247
200+				726	2,370	134
Total > 180	0	0	0	969	4,747	381

[a]Unsorted means no $F_{10.7}$ value was available.

days for which the $F_{10.7}$ flux is missing from the SPIDR database. The database with the topside sounder profiles itself has only the sunspot number as a proxy for the solar activity during each measurement. These profiles cannot be used when the effect of solar activity is investigated, but they are included in all other analyses.

There are two possible biases in the data that one has to keep in mind when interpreting the results. The first possible bias comes from the fact that the peak is assumed to be at the lowest measured point in the profile. Because the satellite measures downward from above the F_2 peak, and the profiles in the database are given by discrete points, it is possible that the lowest point is above the peak, but it can never be below the peak. Because of the data selection procedures discussed above and the way the original data is analyzed [*Jackson*, 1969a, 1969b, 1988], it can be assumed that any bias introduced in this way is small; as said above, this peak is typically 10 km above the true value, even if there are no errors or problems with the profile. The second, and more important, bias results from the varying height of the topside sounders themselves. This is a bias toward lower ion transition levels, and consequentially also toward thinner ionospheres, because a higher transition level has a smaller chance of being measured by the sounders, particularly in the case of the perigee portions of the Alouette 2 and ISIS 1 satellites. Since the transition height itself is correlated with physical parameters like solar and magnetic conditions, this bias must be kept in mind when investigating the influences of these physical drivers on the ionospheric conditions [*Marinov et al.*, 2004]. Because the selection is based on the transition level, the profiles are more likely to be removed from the database when measurements are performed during high solar activity or under disturbed magnetic conditions (cf. Figure 4). This is a result of the transition level being higher in these circumstances and therefore more likely to be above the satellite.

4. Results

For each of the 32,456 profiles left after the cleaning of the database, the integrated error is calculated for the four possible shapes of the profile. The error was the smallest for the exponential profile shape 24,340 times, 74.7% of all cases. Of the remaining profiles, 7302 are best fitted by the α-Chapman curve (accounting for 22.4%), 560 by an Epstein shape, and 381 by the β-Chapman curve. Thus, the conclusion is that no one profile shape can be used universally. The difference between the integrated errors for the Chapman and Epstein profiles is generally smaller than the difference with the exponential shape. The difference between the error for the exponential shape and the one for any of the three others is most of the time an order of magnitude larger than the ones between the Chapman and Epstein profiles. For this reason, and because the Epstein and β-Chapman profiles comprise only a very small fraction of the total number of measured profiles, we mainly concentrate on the difference between profiles that are exponentially shaped and profiles that are not. The precise shape of the nonexponential profiles is thereby ignored.

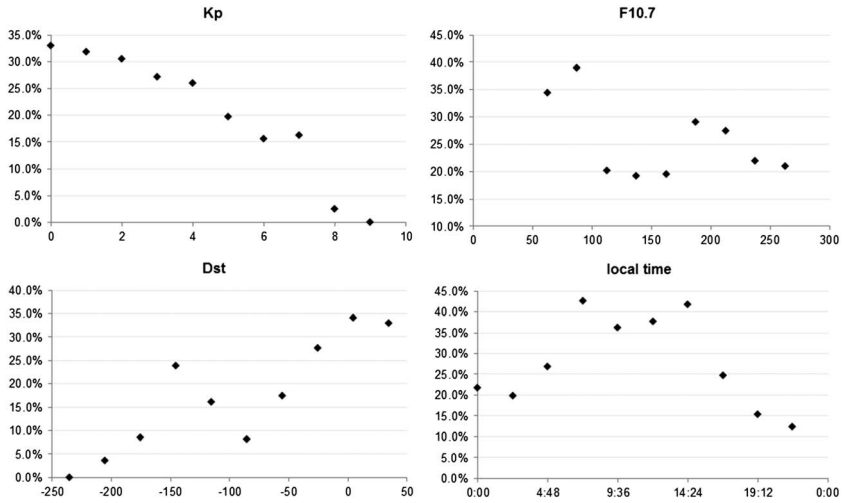

Figure 4. Percentage of profiles containing the transition height, in relation to magnetic *Kp* and *Dst* indices, solar index $F_{10.7}$, and local time.

4.1. Relation to Solar and Magnetic Activity

Since both the solar and magnetic activities are known to heavily influence the ionosphere, it was expected that the indices $F_{10.7}$, *Kp*, and *Dst* can be used to select an appropriate topside profiler, depending on the solar and magnetic conditions. In Table 2, the percentages are given of profiles that are best fitted by the exponential profiler, for different values of the solar and magnetic indices. It seems that the solar activity has some effect on the shape of the topside electron density. For low solar activity, defined as $F_{10.7} < 120$, 75.6% of the profiles have an exponential shape while for high solar activity, $F_{10.7} \geq 180$, this is only 65.9%. Thus, while the expected influence of the solar activity can indeed be seen in the available data, the correlation between the shape of the topside profile and the $F_{10.7}$ index is not sufficient to be used for the selection of an appropriate profiler. There also seems to be a very slight trend toward profiles of nonexponential shapes during disturbed magnetic conditions ($Kp \geq 3$ or $Dst < -0$), although this trend, too, is not clear enough to be useful in the prediction of the topside profile shape. Notice that, due to the selection bias discussed in section 3 and illustrated in Figure 4, the available profiles are unevenly selected over different values of these indices. This makes interpreting the correlations between profile shape and any solar or magnetic index difficult, as any existing correlation with the profile shape might be obscured or amplified by the selection biases.

4.2. Dependency of Profile Shapes on Space and Time

Earlier works [*Marinov et al.*, 2004; *Kutiev and Marinov*, 2007] have already investigated the relation between the scale height and the magnetic coordinates, season, and time of the day. However, as discussed above, this has been done using the regression method to calculate the scale height. As explained earlier, this method can only be used to determine the scale height for a given profiler, not to distinguish between the possible shapes of the profile. This can be done here by calculating the fraction of the profiles best fitted by an exponential curve and by a nonexponential curve as a function of time—day of year as well as time of the day—and magnetic latitude. Solar activity and magnetic disturbances are also expected to have an influence on the shape of the electron density profile. Ideally, this analysis would have to be done separately for different solar activity conditions—measured by the solar 10.7 cm flux—and magnetic conditions—represented by the *Kp* and *Dst* indices. However, due to irregular distribution of data and the stringent data selection procedures described above, the data coverage is insufficient to allow this separation. In particular, there is not enough data available during periods of high solar or

Table 2. Percentages of Profiles Best Fitted by Exponential Profiler, by Solar and Magnetic Indices

$F_{10.7}$		*Kp*		*Dst*	
<120	75.6%	0–2	75.9%	<−50	77.5%
120–180	70.1%	3–4	71.2%	−50–−25	71.5%
≥180	65.9%	4–5	70.4%	≥−25	74.9%
		>5	71.7%		

magnetic activity (this is a consequence of the selection bias illustrated in Figure 4). Because of this, we only perform this analysis for the total data set, without taking into account the solar and magnetic indices.

Figure 5 shows the ratio of nonexponential profiles to exponential ones, for each season, as a function of magnetic latitude and time of the day. Each bin is required to have a minimum of 10 measured density profiles to calculate the ratio of nonexponential to exponential profiles. As a result of the large number of bins, there is still a severe problem with data coverage in this analysis. In order to get at least 10 profiles for most of the bins, those profiles that do not cover the entire topside ionosphere, but are cut off somewhere below the transition level were included here too. The integrated errors for these profiles are calculated over the complete altitude range of the profile. Including these profiles may result in some additional systematic biases, as discussed before, but this is unavoidable in this case. Even when using this larger set of profiles, there are still some bins with insufficient data, as well as large variations in the number of profiles in the other bin. This problem of coverage is a direct result of the nonuniformity of the distribution of profiles in the topside sounder database and the stringent data selection applied [*Verhulst and Stankov*, 2013]. It is unavoidable unless the data selection criteria are made more lenient, and even then the intrinsic irregularities of the data distribution cannot be remediated.

It can be seen from Figure 5 that the considered drivers—magnetic latitude, local time, and season—have some influence on the shape of the profile. For example, at latitudes between 0° and 20°, the ratio is rarely below 0.5, while at higher latitudes, it often goes down to below 0.2. One can also discern some trends with respect to local time and season, although it is impossible to draw any hard conclusion from these. Clearly, these patterns are not so pronounced as to be usable for the selection of an appropriate profiler, at least not without considering other factors that may be of influence. Note that some bins have an extremely large value. This is due to the small number of data included in these bins, resulting in large possible fluctuations in the ratio between the numbers of exponential and nonexponential profiles. These extreme values should be regarded as artifacts of the analysis, rather than physical phenomena. It should also be noted that this ratio has some intermediate value for a lot of bins, meaning there are significant amounts of both exponential and nonexponential profiles. This indicates that there are other factors influencing the shape of the density profiles.

4.3. Relation to Other Profile Characteristics

Figure 6 shows the fraction of profiles that are not exponential in relation to different characteristics of the ionosphere: the F_2 peak height and density, the height of the upper transition level, the thickness of the topside ionosphere—defined as the distance from the F_2 peak to the upper transition level—the scale height at the peak as calculated for an exponential profile shape, and the ratio of the scale heights as calculated for an exponential shape and for an α-Chapman shape. Note that the number of bins used varies between the panels of Figure 6. This results in a higher average number of profiles in histograms with fewer bins.

Evidentially, those parameters are not independent of each other. For example, larger H_{exp} will correlate with larger H_{exp} to H_α ratio. It is therefore expected that the fraction of nonexponential profiles in relation to H_{exp} will be similar to its relation to this ratio of scale heights. This can indeed be seen in Figures 6a and 6b. The same kind of similarity can be seen between Figures 6c and 6d because of the relation between the transition level and the thickness of the ionosphere.

The most obvious relation is the one between the fraction of profiles best fitted by a shape other than the exponential and the scale height calculated assuming an exponential profile. From Figure 6a, it can be seen that the larger the scale height calculated for an exponential profile becomes, the less probable it is that the exponential profile is the best fitting curve. If H_{exp} is smaller than 100 km, the fraction of the profiles for which the exponential curve does not provide the best fit is approximately zero. This fraction sharply increases for larger H_{exp} and is 75% at 250 km. For extremely large values of H_{exp}, 500 km and more, almost all profiles are better fitted with a curve other than the exponential one. The same behavior can be seen in Figure 6b, showing the dependency of the nonexponential fraction of profiles on the ratio between H_{exp} and H_α. Here the transition between almost all exponential profiles and almost no exponential profiles takes place between the ratios of four and six. It should be noted that for any given measured profile, the scale height calculated for an exponential fit is larger than for the α-Chapman fit (the scale heights for Epstein and β-Chapman fits will fall between those two). This is a consequence of the order of densities when the four

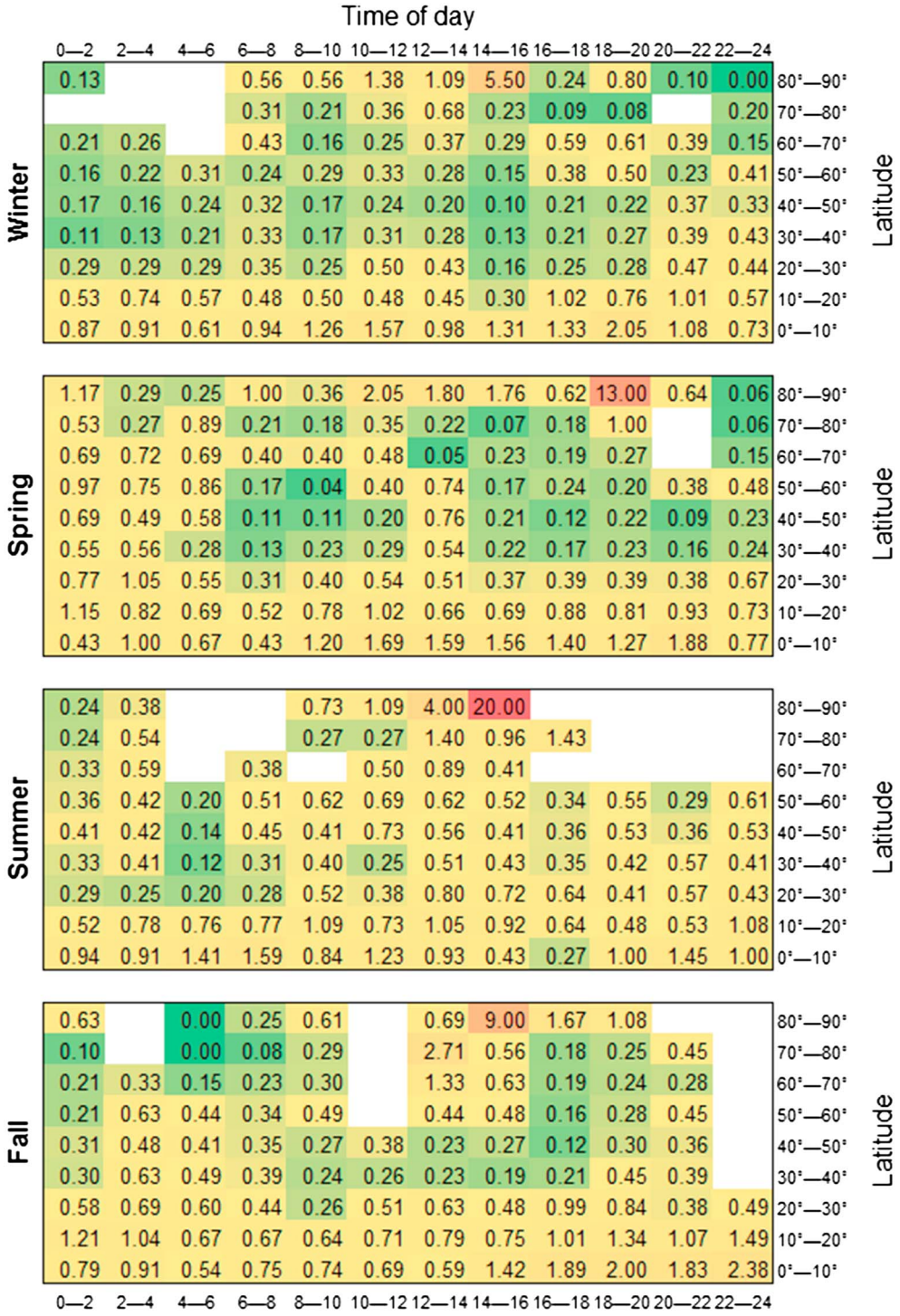

Figure 5. Ratio of profiles best fitted by one of the nonexponential profilers to those best fitted by the exponential profiler, binned by magnetic latitude and local time, for each season. Latitudes belonging to the Northern and Southern Hemispheres are combined, in the appropriate season, ignoring any differences in the ionosphere that probably exist between the hemispheres. In the (geographic) Northern Hemisphere, spring is defined as starting on day of year (DOY) 36 and ending on DOY 127, summer is the interval between DOY 128 and DOY 218, and autumn starts on DOY 219 and ends on DOY 310. Seasons on the Southern Hemisphere are defined using the same intervals for opposite seasons. In this figure, the green color indicates that most profiles are exponential, while the yellow and red mean more profiles are nonexponential. Only those latitude and time bins for which there are at least 10 profiles are considered.

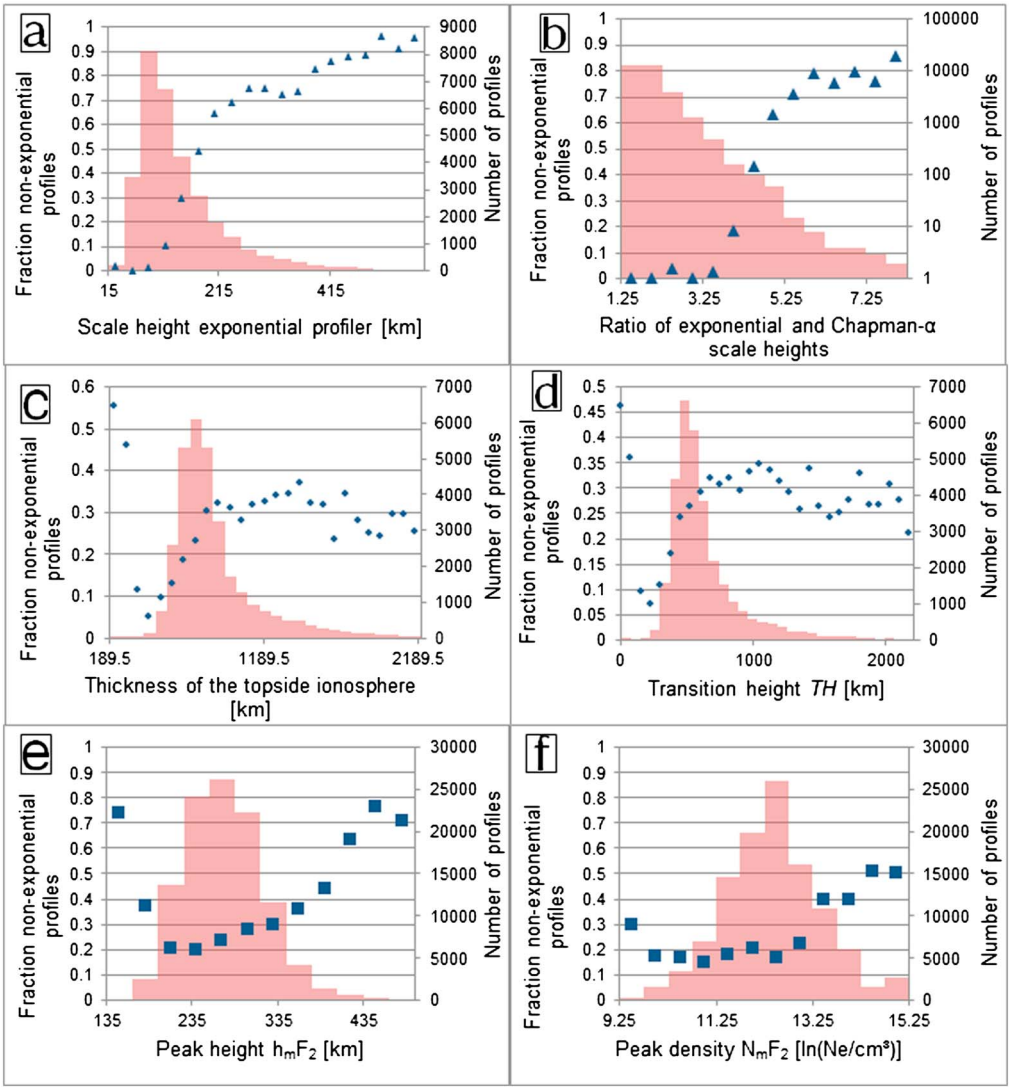

Figure 6. The fraction of nonexponential profiles in relation to different topside characteristics. (a) The relation with the scale height obtained by using the exponential profiler. (b) The relation of the ratio between the scale heights obtained using the exponential and α-Chapman profilers. (c) The relation to the thickness of the ionosphere (the difference between *TH* and h_mF_2). (d) The relation to the transition height itself. (e and f) The relations to peak height h_mF_2 and peak density N_mF_2.

profiles are calculated using the same scale height, as can be seen in Figure 1c. As a consequence, the absolute variation of scale heights is also smaller for α-Chapman fits than it is for exponential fits. This explains why Figures 6a and 6b are almost identical.

Figures 6c and Figure 6d show that there is also a similar relation between the fraction of profiles best described by an exponential curve and the height of the upper transition level and the related thickness of the topside ionosphere. This relation however is not as pronounced as the former. The fraction of profiles that are not exponential grows with larger transition heights but saturates around 30% at transition heights of a thousand kilometers and stays around this level for larger transition heights.

Figures 6e and 6f show the relation of the fraction of nonexponential profiles to the height and density of the F_2 peak. These two characteristics of the ionosphere are also not independent of each other because both are influenced by time of the day, season, solar activity, and geomagnetic conditions. However, the relation between the peak height and density is less straightforward than, for example, the connection between H_{exp} and H_{exp} divided by H_α. Nevertheless, the fraction of nonexponential profiles behaves again similar as a function of these two parameters, increasing with increasing peak heights as well as for increasing peak

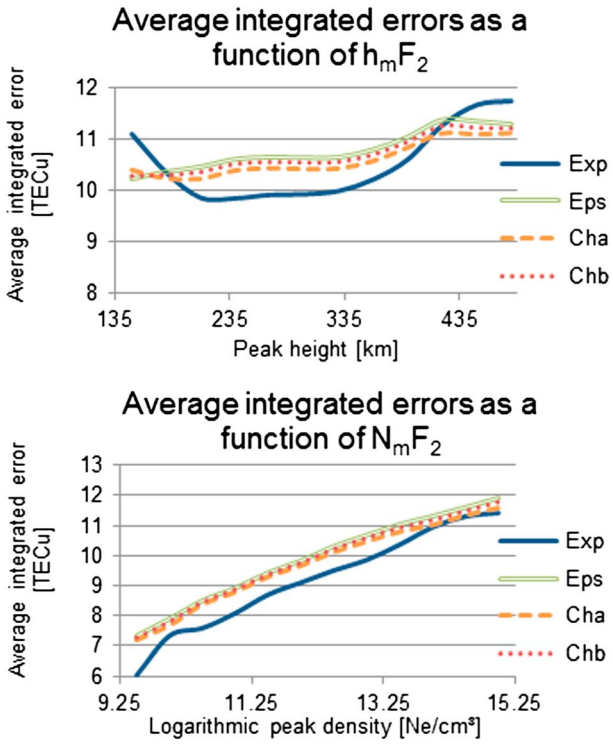

Figure 7. Average integrated error for the best fit obtained using each of the four considered profilers. The error obtained with the Exponential profiler (Exp) is indicated by a solid line, the one obtained using the Epstein curve (Eps) by a double line, and the ones obtained using α-Chapman and β-Chapman functions (Cha and Chb) by dashed lines. (top) The relation between the average integrated errors and the height of the F_2 peak. (bottom) The relation to the peak density.

densities. As a function of the peak density, this fraction climbs from 15% at $\ln(N_e) = 10$ (with N_e in cm^{-3}) to 50%. As a function of F_2 peak height, the percentages increase from 20% to 80% between 200 km and 450 km. For both very small densities and very small peak heights, there is also a sharp increase in the amount of nonexponential profiles. However, there are few measurements available in those ranges so it is possible that this is a result of statistical outliers or some artifact of the data that has not yet been identified in the data cleaning process.

To further clarify the relation between the peak characteristics and the shape of the topside profile, Figure 7 shows the average integrated errors for the four profilers in relation to h_mF_2 and N_mF_2. It is clear from Figure 7 (top) that the height of the F_2 peak can be used to select an appropriate profiler (notice that the scale on the vertical axis is logarithmic; the differences in errors are therefore large). For values of h_mF_2 between about 190 km and 400 km, the error when using the exponential profiler is an order of magnitude lower than for any of the other three. However, for higher or lower values of the peak height, the α-Chapman profiler is much better. In fact, the errors associated with the exponential profiler quickly become an order of magnitude larger than those of all three other profilers. For extremely low values of the peak height, the Epstein profiler gives an even better fit than the α-Chapman, but the differences in errors between these two is never very large, and there are relatively few profiles with such small h_mF_2, so this seems to be not significant. Regarding the peak density, it is obvious that the average errors become equal for all profiles with high densities.

However, the fact that the average errors become equal for large N_mF_2 does not imply that for each individual profile, the different theoretical shapes produce equally good approximations. In Figure 8a, it can be seen that the difference in Er_i between the fit obtained with the exponential profiler (Er_{exp}) and the one obtained using the best fitting nonexponential profiler (Er_n) does not approach zero for large values of N_mF_2. Rather, the average errors become equal because the distribution of $Er_{exp} - Er_n$ becomes symmetrical around zero for high peak densities. In fact, the average absolute value of the differences in absolute error (Figure 8b) increases with N_mF_2, although the relative error (Figure 8d) does slightly decrease. For low peak densities, it can be seen, most clearly in Figure 8c, that using a nonexponential profiler can produce errors much larger than using the exponential one, even if for some individual profiles, the best fit is obtained with one of the nonexponential profilers. Using these results to select an appropriate topside profiler therefore guarantees that the errors made, on average, will be minimal, even if not every individual profile is approximated with the optimal shape.

4.4. Relations Between Topside Characteristics

Apart from the shape of the profile, the topside electron density is characterized by three important parameters: N_mF_2, h_mF_2, and UTL. Another important characteristic derived from these parameters is the thickness of the topside ionosphere, i.e., the difference between the transition height and the peak height. In the previous section, it was shown that these parameters provide the best indication about the appropriate

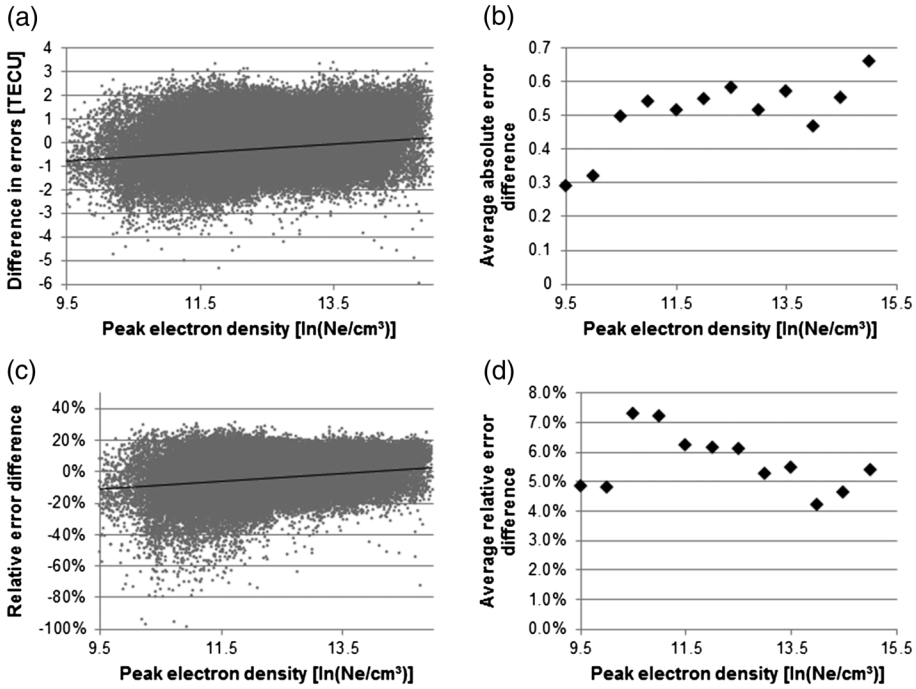

Figure 8. Differences between the (a and b) absolute and (c and d) relative errors obtained by exponential profiler and best fitting nonexponential profiler, in function of peak density N_mF_2. Figures 8a and 8c show all profiles as well as the linear trend line. Figures 8b and 8d show the averages, for each density bin, of the absolute values in Figures 8a and 8c.

profiler to use for the topside. It is important therefore to realize that those characteristics are not entirely independent of each other. In Figure 9, the relations between the three fundamental characteristics are shown. Clearly, there are correlations between h_mF_2 and UTL and between h_mF_2 and N_mF_2 but not between N_mF_2 and UTL. It should be noted that these relationships are influenced by the data selection, for example, very high values of UTL are less likely to occur because the chance of the satellite being above it is small. The relation between peak height and peak density was also investigated without the requirement of UTL falling within the measured profile. It was found that this requirement introduces a slight bias toward the lower and denser peaks, but the shape of the distribution in Figure 9 (top) remains the same.

5. Discussion

There is one important factor contributing to the discrepancies between the observation data and the theoretical functions applied here: the assumption of constant scale height. The assumption of constant ion/plasma scale height is a bit restrictive because the scale height depends on the ion/plasma temperature which is variable with altitude. However, in the lower topside ionosphere (a couple of hundred kilometers above h_mF_2), the plasma scale height varies only slowly with altitude [*Reinisch and Huang*, 2001]. Some studies using variable scale heights have already been done [*Reinisch et al*., 2007; *Nsumei et al*., 2012], but so far they consider exclusively the α-Chapman profiler. A better approach could be to combine the use of different profilers with variable scale heights and determine the ones that provide the best fit for the particular geophysical conditions. This will become feasible when more topside ionosphere measurements become available.

The inherent problems of the database discussed above are another possible source of such discrepancies. Improvements to the results might be obtained by repeating the analysis presented here using the database of profiles scaled by the topside ionogram scaler with true height (TOPIST) software [*Bilitza et al*., 2004; *Benson et al*., 2012]. The TOPIST program provides continuous traces of electron density in relation to height, scaled from the topside ionograms. Some error sources, discussed in the previous sections, are expected to be less important for these data.

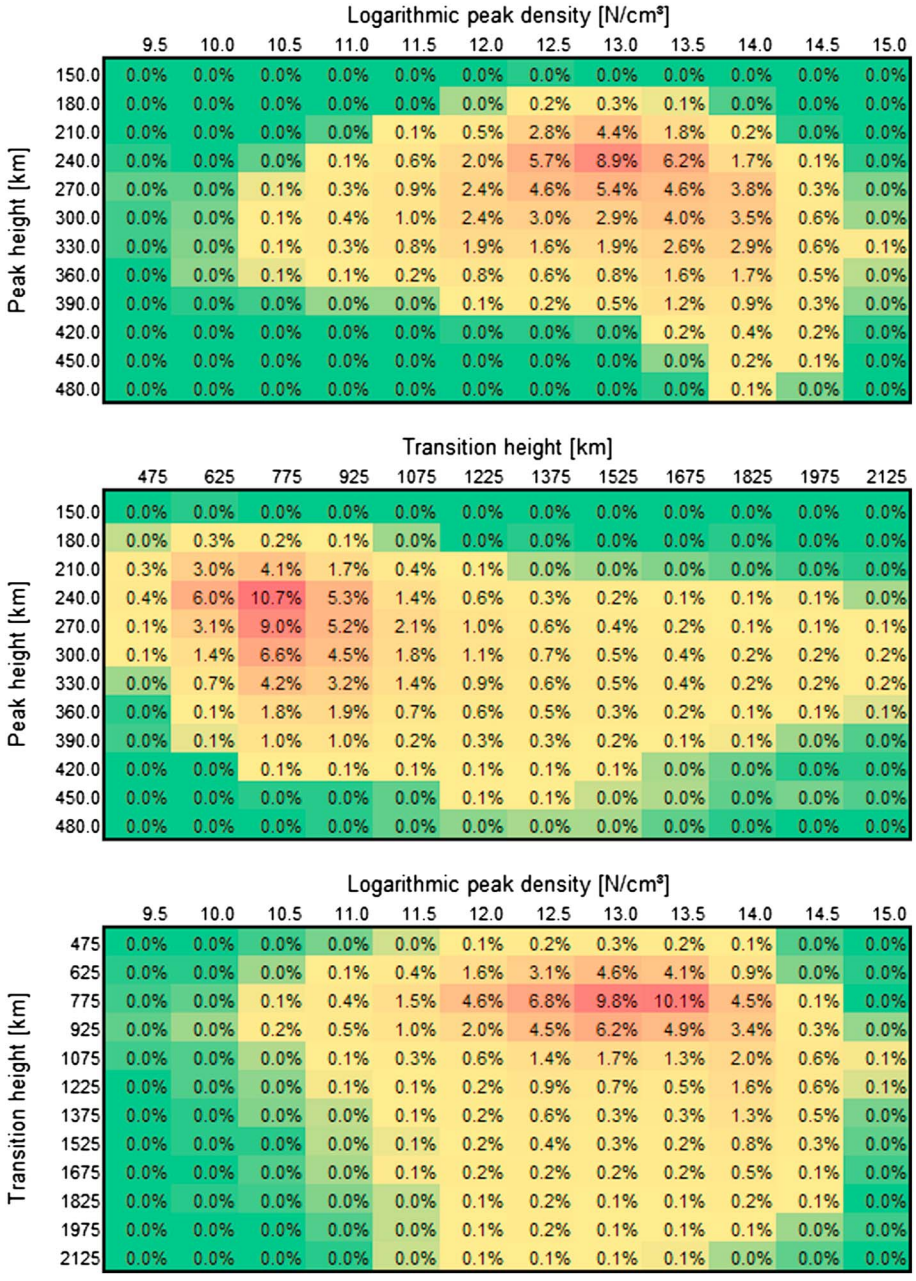

Figure 9. Relations between the topside characteristics peak height h_mF_2, peak density N_mF_2, and upper transition height *TH*. Given are the percentages of profiles, in the cleaned data set, that fall in each bin. (top) A clear relationship between peak height and peak density. (middle) The peak height correlated to the transition height. (bottom) The peak height does not correlate in the case of the peak density.

Also, by combining parts of different shapes into one model, following the approach of *Booker* [1977]. It can be seen from Figure 2 that the α-Chapman curve fits the measured electron densities very well from the F_2 peak up to a height of about 400 km. However, the upper transition level for this particular profile is calculated to be at 750 km. To get a better fit for this profile between 400 km and the upper transition level, an exponential curve could be used, with a separately calculated scale height. In this manner, the topside ionosphere can in general be divided in two or more layers for which different shapes are used to model them. The details of how such a combination of differently shaped parts can be used to get the best fit for each profile will be the subject of a further study.

The solar and geomagnetic activity have a crucial influence on the profile shape and the ionospheric dynamics in general, but the commonly used activity indices do not provide much useful information and criteria to select a particular profiler. The same holds true for local time, season, and magnetic latitude/longitude. Especially, the season seems to play an important role. More obvious relations exist between the profile shape and the other characteristics of the topside ionosphere, especially the height of the F_2 peak (see Figures 6e and 7) and the scale height (see Figures 6a and 6b). To select an appropriate profiler in applications, for example, LIEDR, it is therefore better to rely on these measured characteristics rather than the external indices describing the ionospheric drivers.

There are two possible explanations for the failure of the commonly used indices to provide directly the optimal choice of profiler. First, the fact that there are many drivers (solar and geomagnetic activity, season, time of the day, and magnetic latitude and longitude) that simultaneously influence the ionospheric behavior makes it difficult to determine the influence of each driver separately. Second, some indices describing those drivers (e.g., the *Kp* and *Dst* indices) are averaged over an extended time or region which renders them unsuitable for proper determination of the optimal profile to be used locally and in high-time resolution applications like LIEDR. For example, the *Kp* index is a planetary index (value obtained from a dozen observatories worldwide), and $F_{10.7}$ is only calculated once a day from measurements at one location.

The influences of the physical drivers are of course still taken into account when using the peak characteristics to determine the profiler to be used, albeit indirectly, because they have major influences on these characteristics.

6. Conclusion

Four well-known analytical ionospheric profilers (Exponential, α-Chapman, β-Chapman, and Epstein) have been evaluated using topside electron density profiles based on earlier manual scaling of topside sounder ionograms. The following conclusions can be drawn:

First and foremost, the accumulated topside sounder database proved to be a valuable source of information when investigating the composition and complex dynamics of the upper ionosphere, for development and evaluation of theoretical and empirical models. However, a special attention must be paid to proper data screening and preprocessing of the database. A study similar to this one is currently underway using the TOPIST data, which is expected to need less cleaning and preprocessing.

It has been established that, in order to adequately model the topside ionospheric plasma distribution with the help of these profilers, it is necessary to use different scale heights for the different profile shapes in use.

The analysis shows that in almost 75% of the cases, the best fit is provided by the exponential profiler, and in the rest of the cases, the best fit is mainly by the α-Chapman profiler. This is due in part to problems with the data—which will be less of an issue in the follow up study using the TOPIST data—and in part due to physical effects, as discussed in section 5.

One very important finding is that the best indication for the selection of a profiler comes from the ionospheric density peak characteristics (N_mF_2 and h_mF_2), rather than from "external" parameters such as solar/geomagnetic indices, season, and local time. For real-time applications, such as LIEDR, this is a very useful result because the peak characteristics can be measured locally and provided immediately by a ground-based ionosonde.

Acknowledgments
This work is funded by the Royal Meteorological Institute via the Belgian Solar-Terrestrial Centre of Excellence. The topside sounder data are provided by the U.S. National Space Science Data Center and the solar/geomagnetic activity indices are from the U.S. National Oceanic and Atmospheric Administration.

References

Benson, R. F. (2010), Four decades of space-borne radio sounding, *Radio Sci. Bull.*, *333*, 24–44.
Benson, R. F., V. Truhlik, X. Huang, Y. Wang, and D. Bilitza (2012), Improving the automatic inversion of digital Alouette/ISIS ionogram reflection traces into topside electron density profiles, *Radio Sci.*, *47*, RS0L04, doi:10.1029/2011RS004963.
Bilitza, D. (2001), International Reference Ionosphere 2000, *Radio Sci.*, *36*, 261–275.
Bilitza, D., and B. Reinisch (2008), International Reference Ionosphere 2007: Improvements and new parameters, *Adv. Space Res.*, *42*(4), 599–609.
Bilitza, D., B. Reinisch, R. Benson, J. Grebowsky, N. Papitashvili, X. Huang, W. Schar, and K. Hills (2003), Online data base of satellite sounder and *In-situ* measurements covering two solar cycles, *Adv. Space Res.*, *31*, 769–774.
Bilitza, D., X. Huang, B. D. Reinisch, R. F. Benson, H. K. Hills, and W. B. Schar (2004), Topside ionogram scaler with true height algorithm (TOPIST): Automated processing of ISIS topside ionograms, *Radio Sci.*, *39*, RS1S27, doi:10.1029/2002RS002840.

Booker, H. G. (1977), Fitting of multi-region ionospheric profiles of electron density by a single analytical function of height, *J. Atmos. Terr. Phys.*, *39*, 619–623.
Coïsson, P., S. M. Radicella, R. Leitinger, and B. Nava (2006), Topside electron density in IRI and NeQuick: Features and limitations, *Adv. Space Res.*, *37*, 937–942.
Corless, R. M., G. H. Gonnet, D. E. G. Hare, D. J. Jeffrey, and D. E. Knuth (1996), On the Lambert W function, *Adv. Comput. Math.*, *5*, 329–359.
Depuev, V. H., and S. A. Pulinets (2004), A global empirical model of the ionospheric topside electron density, *Adv. Space Res.*, *34*, 2016–2020.
Fonda, C., P. Coïsson, B. Nava, and M. Radicella (2005), Comparison of analytical functions used to describe topside electron density profiles with satellite data, *Ann. Geophys.*, *48*, 491–495.
Hargreaves, J. K. (1992), *The Solar-Terrestrial Environment*, Cambridge Univ. Press, Cambridge, U. K.
Jackson, J. E. (1969a), The reduction of topside ionograms to electron-density profiles, *Proc. IEEE*, *57*, 960–976.
Jackson, J. E. (1969b), Comparisons between topside and ground-based soundings, *Proc. IEEE*, *57*, 976–985.
Jackson, J. E. (1988), Results from Alouette 1, Explorer 20, Alouette 2 and Explorer 31, NSSDC Report 88-10, National Space Science Data Center, Greenbelt, Md.
Jackson, J. E., and E. S. Warren (1969), Objectives, history, and principal achievements of the topside sounder and ISIS programs, *Proc. IEEE*, *57*, 861–865.
Jackson, J. E., E. R. Schmerling, and J. H. Whitteker (1980), Mini-review on topside sounding, *IEEE Trans. Antennas Propag.*, *AP-28*, 184–288.
Kutiev, I., and P. Marinov (2007), Topside sounder model of scale height and transition height characteristics of the ionosphere, *Adv. Space Res.*, *39*, 759–766.
Marinov, P., I. Kutiev, and S. Watanabe (2004), Empirical model of O^+-H^+ transition height on topside sounder data, *Adv. Space Res.*, *34*, 2021–2025.
Nsumei, P., B. W. Reinisch, X. Huang, and D. Bilitza (2012), New Vary-Chap profile of the topside ionosphere electron density distribution for use with the IRI model and the GIRO real time data, *Radio Sci.*, *47*, RS0L16, doi:10.1029/2012RS004989.
O'Loughlin, K. L. (1997), SPIDR on the Web: Space Physics Interactive Data Resource on-line analysis tool, *Radio Sci.*, *32*(5), 2021–2026.
Rawer, K. (1988), Synthesis of ionospheric electron density profiles with Epstein functions, *Adv. Space Res.*, *8*(4), 191–198.
Rawer, K. (1993), *Wave Propagation in the Ionosphere*, Kluwer Academic Publishers, Dordrecht, The Netherlands.
Reinisch, B. W. (1996), Modern ionosondes, in *Modern Ionospheric Science*, edited by H. Kohl et al., pp. 440–458, European Geophysical Society, Katlenburg-Lindau.
Reinisch, B. W., and X. Huang (2001), Deducing topside profiles and total electron content from bottomside ionograms, *Adv. Space Res.*, *27*(1), 23–30.
Reinisch, B. W., X. Huang, I. A. Galkin, V. Paznukhov, and A. Kozlov (2005), Recent advances in real-time analysis of ionograms and ionospheric drift measurements with digisondes, *J. Atmos. Sol. Terr. Phys.*, *67*(12), 1054–1062.
Reinisch, B. W., P. Nsumei, X. Huang, and D. K. Bilitza (2007), Modeling the F_2 topside and plasmasphere for IRI using IMAGE/RPI and ISIS data, *Adv. Space Res.*, *39*(5), 731–738.
Stankov, S. M., N. Jakowski, S. Heise, P. Muhtarov, I. Kutiev, and R. Warnant (2003), A new method for reconstruction of the vertical electron density distribution in the upper ionosphere and plasmasphere, *J. Geophys. Res.*, *108*(A5), 1164, doi:10.1029/2002JA009570.
Stankov, S. M., K. Stegen, P. Muhtarov, and R. Warnant (2011), Local ionospheric electron density profile reconstruction in real time from simultaneous ground-based GNSS and ionosonde measurements, *Adv. Space Res.*, *47*(7), 1172–1180.
Titheridge, J. E. (1976), Ion transition heights from topside electron density profiles, *Planet. Space Sci.*, *24*, 229–245.
Verhulst, T., and S. M. Stankov (2013), The topside sounder database – Data screening and systematic biases, *Adv. Space Res.*, *51*, 2010–2017.
Webb, P. A., R. Benson, and J. Grebowsky (2006), Altitude variations of middle-latitude topside ionospheric electron-density profiles, *Adv. Space Res.*, *37*, 951–957.